Bauschinger effect in unpassivated freestanding thin films

Shishvan, Siamak Soleymani; Nicola, Lucia; Van der Giessen, Erik

Published in:
Journal of Applied Physics

DOI:
10.1063/1.3407505

Publication date:
2010

Bauschinger effect in unpassivated freestanding thin films

Siamak Soleymani Shishvan,[1,a)] Lucia Nicola,[2] and Erik Van der Giessen[3,b)]
[1]*Department of Structural Engineering, University of Tehran, P.O. Box 11365-4563, Tehran, Iran*
[2]*Department of Materials Science and Engineering, Delft University of Technology, Mekelweg 2, 2628 CD Delft, The Netherlands*
[3]*Department of Applied Physics, Zernike Institute for Advanced Materials, University of Groningen, Nyenborgh 4, 9747 AG Groningen, The Netherlands*

(Received 31 December 2009; accepted 8 March 2010; published online 10 May 2010)

Two-dimensional (2D) discrete dislocation plasticity simulations are carried out to investigate the Bauschinger effect (BE) in freestanding thin films. The BE in plastic flow of polycrystalline materials is generally understood to be caused by inhomogeneous deformation during loading, leading to residual stress upon unloading. This inhomogeneity can be caused by dislocation pile-ups, variations in texture, grain orientations, and grain size. To study the BE, columnar-grained films as well as films with multiple grains across the thickness are considered. The film is modeled in a 2D framework by a unit cell consisting of an array of grains with different orientation. In order to capture the interaction among grains, we motivate and explore the use of an affine deformation assumption on the grain level to mimic the three-dimensional geometry in this framework. It is shown that the dispersion of grain size in a film together with the size-dependence of yield strength leads to significant BEs in bare films. Quantitative comparison of simulations with experimental data is provided. © *2010 American Institute of Physics*. [doi:10.1063/1.3407505]

I. INTRODUCTION

Experimental evidence that strained freestanding thin metal films can exhibit a pronounced Bauschinger effect (BE) upon unloading was presented first by Xiang and Vlassak.[1] They tested passivated and unpassivated copper films with a columnar grain structure. In passivated films, a hysteresis cycle was observed during loading, unloading, and reloading. Unpassivated films, however, showed no reverse plasticity upon full unloading. These results were rationalized in terms of dislocation mechanics: the presence of a strong interface between metal film and passivation layer prevents the dislocations from gliding out of the film. The elastic energy stored into the dislocation pile-ups promotes reversed plasticity during unloading when the film is still in tension.

By contrast, recent experiments by Rajagopalan *et al.*[2] have shown that early reversed plasticity takes place also upon unloading of unpassivated thin films. Their films were very thin (about 200 nm) freestanding unpassivated aluminum and gold films with a few grains across the film thickness. The sets of films tested by Xiang and Vlassak[1] and Rajagopalan *et al.*[2] differ in terms of material, film thickness as well as grain size. The copper films in Ref. 1 are thicker (more than 300 nm) and predominantly have columnar grains. It is also noteworthy that the unpassivated films tested in Ref. 2 show considerable strain hardening upon loading, contrary to those in Ref. 1.

It has been widely recognized that the response of a thin film depends not only on the grain size, just as in bulk polycrystalline materials, but also on the film thickness. Such size effects can only be captured by plasticity models with a material length scale, such as enriched continuum models or models using discrete dislocation plasticity (DDP). The latter owes this ability to capture size effects to the fact that, while adopting a continuum description of the elastic lattice, it retains individual dislocations as carriers of plastic deformation. Fertig and Baker[3] recently presented a review of modeling dislocations in thin films via analytical techniques, as well as two-dimensional (2D) and three-dimensional (3D) DDP simulations.

We here study the origin of the BE in thin films by means of a 2D DDP model. Films are represented by an array of grains having different orientations, with plastic deformation being represented by the motion of discrete dislocations that get either blocked by the grain boundaries (GBs) or escape from free surfaces. Thus, the model explicitly incorporates the effects of grain size and orientation, as well as the piling-up of dislocations, which gives rise to size dependent plastic flow as shown previously for passivated films in Ref. 4. A recent innovation of the model in Ref. 4 is the introduction of a 2D constitutive rule to represent Frank–Read sources, taking into account that the grain size limits the available and effective dislocation source length and thereby its strength.[5]

As a follow-up to Ref. 4, we will demonstrate here that this dislocation plasticity framework can also capture early reversed plasticity in unpassivated films with just one or a few grains across the thickness. To augment the present 2D framework with consideration of the 3D film microstructure, the use of an affine deformation assumption on the grain level is proposed. It is shown that the variation in grain size in a film is key to considerable BEs in unpassivated thin

[a)]Also at Zernike Institute for Advanced Materials, Dept. of Applied Physics, University of Groningen, Nyenborgh 4, 9747 AG Groningen, The Netherlands.
[b)]Electronic address: e.van.der.giessen@rug.nl.

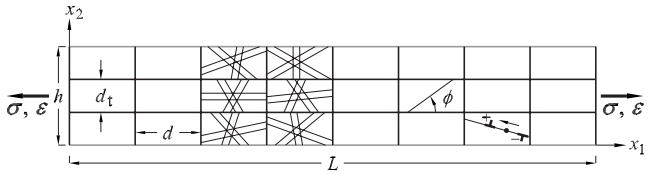

FIG. 1. Plane-strain model of an unpassivated freestanding thin film in tension, illustrating slip systems, a source, and the sign convention for dislocations. The film shown has three grains across the thickness, but simulations are also carried out for columnar-grained and two-layer films.

films, especially in ones with columnar grains. Before presenting the results and their comparison with experiments, the computational methodology is presented.

II. METHOD

Polycrystalline thin films of thickness h are modeled as 2D arrays of rectangular grains of height d_t and width d, as shown in Fig. 1. The film thickness h and grain height d_t are interrelated through $h=nd_t$, where n is the number of grains across the thickness (number of layers). Each grain has three slip systems, with slip planes oriented at ϕ, $\phi+60°$, and $\phi+120°$ from the loading direction. The orientation of each grain, ϕ, is different for all grains and chosen at random. Consistent with the plane-strain conditions perpendicular to the plane of observation, all dislocations are of edge character and have a Burgers vector magnitude b. All GBs are assumed to be impenetrable to dislocations, while dislocations can freely leave through the top and bottom surfaces since they are unpassivated. Periodic boundary conditions are used to prescribe the tensile deformation, and the top and bottom surfaces of the film are traction free. The boundary conditions are imposed by way of the superposition method of Van der Giessen and Needleman.[6] Tension is imposed by a prescribed displacement difference between unit cells of length L, i.e.,

$$u_i(L,x_2) = u_i(0,x_2) + L\varepsilon(t)\delta_{i1}, \quad i=1 \text{ and } 2, \tag{1}$$

where $\varepsilon(t)$ is the imposed strain as a function of time and δ_{ij} is the Kronecker delta. A more complete description of the analysis and further references are given in Ref. 4. It is noted that to prevent extensive bending of the film due to nonuniform plastic deformation, the following condition is imposed along the mid-plane of the film

$$u_2(x_1,h/2) = 0, \tag{2}$$

to represent the constraints imposed by the grains in front of and behind those represented in 2D.

Dislocations are modeled as line defects in a linear elastic solid, so that their long-range interactions are directly accounted for. Short-range interactions are incorporated through a set of constitutive rules that intend to represent key dislocation mechanisms: the nucleation, glide, and annihilation of dislocations as well as their pinning at obstacles. From the stress field in a given state of applied strain and for the current dislocation structure, the Peach–Koehler force on each dislocation is computed, which subsequently determines its glide motion. The Peach–Koehler force also controls the nucleation of dislocations through a 2D version of the Frank–Read source, as proposed in Ref. 6; namely, a point that generates a dipole of edge dislocations when the Peach–Koehler force at the source exceeds the source strength $b\tau_{nuc}$ during a time span t_{nuc}. The sign of the dipole is determined by the direction of the Peach–Koehler force.

Sources are randomly distributed over the potentially active slip planes with a given density ρ_{nuc}, and the value of τ_{nuc} of each source is determined randomly from a distribution that reflects that the segments forming a Frank–Read source in 3D have different lengths. Following Ref. 6, Nicola *et al.*[4] assumed a normal distribution for the source strength (yet, independent of the film microstructure), and fitted the average source strength and the density of sources to an experimental result from Ref. 1 and achieved quantitative agreement for the predicted yield strength of thin films. We refer to this method as *grain-size independent source strength model* in the sequel. Shishvan and Van der Giessen[5] have recently refined this approach by explicitly taking into account that the grain size limits the available and effective dislocation source length and thereby its strength. In this so-called *grain size dependent source strength model*, the value of τ_{nuc} of each source is determined by

$$\tau_{nuc} = \tau_{nuc}^0 + \tau_{nuc}^{LN}, \tag{3}$$

where τ_{nuc}^{LN} is picked randomly from a log-normal distribution which is bounded by the theoretical strength of the material and by a minimum strength that depends on the film thickness and grain size as described in detail in Appendix A. The τ_{nuc}^0 is a material-dependent constant that is meant to capture the effect of obstacles and other confinement effects on the operation of Frank–Read sources. The value of the latter along with the density of sources ρ_{nuc} is to be fitted to an experimental stress-strain curve of a film with a chosen thickness. The method has been presented in Ref. 5 and applied to predict the stress-strain curves for two independent sets of Cu films.[1,7] After fitting the free parameters to one of the experimental curves, all other curves were predicted and excellent agreement was found with the experimental results, both in terms of yield strength and hardening rate.

In general, dislocations can be blocked by point obstacles, which represent forest dislocations on intersecting slip planes or small precipitates, but we will assume such obstacles are not present in the thin films considered here. Grain boundaries, however, may provide strong obstacles to dislocation motion. While rules for dislocation transmission across tilt GBs are being developed (see, e.g., Ref. 8), for simplicity we here assume them to be impenetrable. Several aspects of dislocation plasticity as well as properties of GBs are admittedly missing in the present 2D model. Nevertheless, the simulations in Refs. 4 and 5 have shown that quantitative agreement can be obtained with the experimental stress-strain response of thin films in tension.

III. NUMERICAL RESULTS

Just as in earlier studies,[4,5] we adopt material parameters representative of copper: $\nu=0.34$, $E=110$ GPa ($\mu=41$ GPa), $b=0.25$ nm, and $B=10^{-4}$ Pa s. The nucleation properties—ρ_{nuc} and τ_{nuc}—are the only free material param-

eters. For the grain-size independent source strength model, we follow Ref. 4 in adopting $\rho_{\text{nuc}}=15\ \mu\text{m}^{-2}$ and in randomly selecting the strength τ_{nuc} of each source from a Gaussian distribution with an average of 100 MPa and standard deviation of 20 MPa. For the grain size dependent source strength model, the parameter values fitted to the experiments by Xiang and Vlassak[1] are: $\tau_{\text{nuc}}^{0}=0.43\times10^{-3}E$ and $\rho_{\text{nuc}}=30\ \mu\text{m}^{-2}$.[5] It is worth emphasizing, however, that the former model requires that ρ_{nuc}=constant, while the latter model needs $\rho_{\text{nuc}}\propto 1/d$ for different film thickness/grain size. The above mentioned value for ρ_{nuc} was fitted for a 1 μm thick film with grain size $d=1.5\ \mu$m. For more details, we refer to Ref. 5.

We use eight grains in the periodic cell, and assume that the film is initially stress free, and dislocation free, as in Refs. 4 and 5. To reduce statistical effects, various realizations of grain orientation, source locations, and random source strengths are considered for each case. The corresponding results are averaged and the scatter caused by the different realizations is shown as an error bar. The number of realizations is chosen such that adding a new realization result yields a negligible change to the averaged response.

A comparison of the predictions by the two nucleation models is shown in Fig. 2. Both a 1 μm thick Cu film with a grain size of $d=1.5\ \mu$m and a thinner $h=0.34\ \mu$m film with a grain size of $d=0.33\ \mu$m, studied in Ref. 1 are modeled. For the thicker film, good agreement of the simulated results with the experimental curve is found [Fig. 2(a)] for both models; this is less so for the thinner one, where an early onset of plasticity with a very high hardening rate is predicted by the grain size independent source strength model [Fig. 2(b)]. This illustrates that the size dependence of yield and hardening is not only governed by the available dislocation glide distance and the development of back stress associated with the piling-up of dislocations against GBs but is also partly due to the distribution of the source strengths. It has been shown that the size-dependent plasticity in thin films is governed mainly by source limitation mechanism as the film thickness/grain size decreases.[5] To study the BE in thin films, the grain size dependent source strength model is adopted in the sequel.

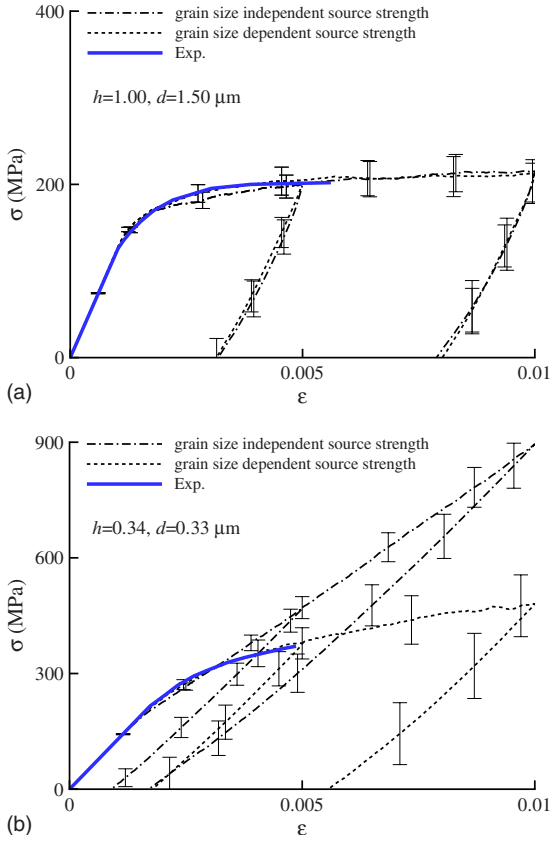

FIG. 2. (Color online) Comparison of the predictions of grain size independent source strength DDP model (Ref. 4) and size dependent source strength DDP model (Ref. 5). Stress-strain curves for (a) 1 μm and (b) 0.34 μm thick film. For comparison purposes, the experimental stress-strain curves from Xiang and Vlassak (Ref. 1) are included.

TABLE I. Characteristics of the simulated films. [It is noted that the definition of $\rho_{\text{GB}}^{(n)}$ in Ref. 9 is based on consideration of a 2D film, while in defining the ratio of free surface to GB area (Ref. 2) considered columns of 3D grains of dimension $d\times d\times d_t$.]

h [a]	n [a]	d_t [a]	d [a]	AR[b]	$\rho_{\text{GB}}^{(n)}$ [c]	Free surface to GB area[d]
1.00	1		1.00	1.00	1.00	0.50
1.00			1.50	0.67	0.67	0.75
0.75			0.44	1.70	2.27	0.29
0.34			0.33	1.03	3.03	0.49
0.25			0.37	0.68	2.70	0.74
0.20			0.38	0.53	2.63	0.95
1.50	2	0.75	0.44	1.70	2.94	0.13
1.00		0.50	0.50	1.00	3.00	0.20
0.50		0.25	0.37	0.68	4.70	0.27
0.40		0.20	0.38	0.53	5.13	0.32
1.00	3	0.33	0.33	1.00	5.03	0.12
0.75		0.25	0.37	0.68	5.37	0.17
0.60		0.20	0.38	0.53	5.96	0.19

[a]For definitions, see Fig. 1; all dimensions are in μm.
[b]Aspect ratio of the grains, h/d or d_t/d.
[c]Density of GBs, defined as (Ref. 9): $\rho_{\text{GB}}^{(n)}=(1/d)+(n-1)/n(1/d_t)$ (in μm^{-1}).
[d]Free surface to GB area, defined as (Ref. 2): $d/[2h+(n-1)d]$.

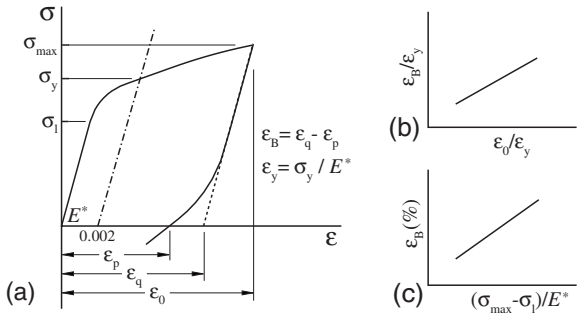

FIG. 3. (a) Schematic representation of the BE in a thin film. (b) and (c) Two common representations of the BE measure used also in the present study.

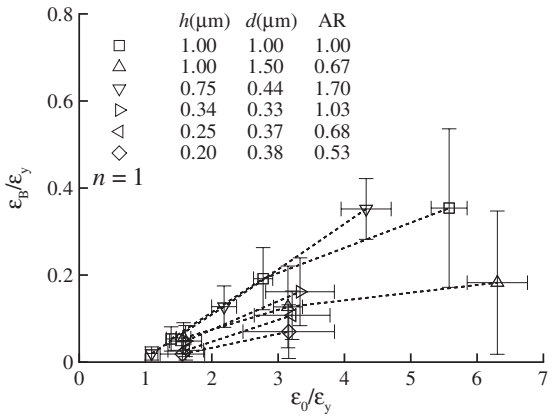

FIG. 4. ε_B as a function of prestrain ε_0, both normalized by the yield strain as defined in the inset of Fig. 3, for columnar-grained films unloaded from $\varepsilon_0=0.005$ and 0.01. Films with thickness 1 and 0.75 μm have been unloaded from $\varepsilon_0=0.0025$. Dashed lines are drawn as a guide to the eye.

A. Predicted BE

A wide range of thin films with thickness between 0.2 and 1.5 μm containing one to three grains across the thickness and grain size from 0.33 to 1.5 μm is considered in this study; the parameter set is summarized in Table I.

The BE as observed in a loading-unloading cycle can be characterized in different ways, as illustrated in Fig. 3. The key quantity is the BE strain ε_B, defined as the difference between the actual residual strain ε_p and the hypothetical residual strain ε_q if unloading were purely elastic [see Fig. 3(a)]. In the literature, ε_B is presented as a function of either the applied prestrain ε_0[1,4] or the ratio $(\sigma_{max}-\sigma_l)/E^*$.[2] Here, σ_l is the elastic limit stress, defined as the point in the stress-strain curve where the secant modulus is equal to 95% of the plane-strain elastic modulus E^*. Plotting ε_B against $(\sigma_{max}-\sigma_l)/E^*$ is inspired by the fact that the latter contains information about the amount of hardening, something that is supposedly strongly linked to the BE. Often ε_B is normalized by the yield strain ε_y corresponding to the 0.2% yield stress σ_y. Figures 3(b) and 3(c) schematically show the experimental trends for these two representations, respectively.

First we analyze the results for the columnar-grained $(n=1)$ films of Table I. Figure 4 shows the variation in the value of $\varepsilon_B/\varepsilon_y$ as a function of the normalized prestrain $\varepsilon_0/\varepsilon_y$, computed for unloading from prestrains of $\varepsilon_0=0.0025$, 0.005, and 0.01. It is seen that there is no or little BE for $\varepsilon_0/\varepsilon_y \lesssim 1.5$, which is in good agreement with the experimental results of Xiang and Vlassak[1] for unpassivated films. Yet, for larger $\varepsilon_0/\varepsilon_y$, the BE seems to increase with increasing prestrain; this trend has indeed been observed in Refs. 1 and 4 but for passivated films, while here the films are bare.

Closer examination of the results in Fig. 4 reveals that for a fixed, relatively high value of $\varepsilon_0/\varepsilon_y$, the BE is stronger when the grain aspect ratio $AR=h/d$ is larger. The Bauschinger strain ε_B remains low for pancakelike grains with small AR, whereas it attains 20% or more of the yield strain when the grains are equiaxed or even needlelike $(AR \gtrsim 1)$. These observations link-up with findings in previous DDP studies of thin films under tension[4,9] that needlelike grains exhibit a high hardening rate due to the development of dislocation pile-ups against GBs. These pile-ups are responsible for the storage of energy, which assists reverse plastic deformation during unloading. Dislocation pile-ups are much less favorable in pancakelike grains, which therefore harden less and exhibit a smaller BE. Also, it is worth noting that films with small grains do not contain long pile-ups, simply because of size limitations. This implies that the BE in such films does not depend directly on pile-up length, but on the number of pile-ups in a grain and on the spacing between dislocations in a pile-up. Also, it should be noted that the development of pile-ups is coupled not only to the presence of GBs but also to the presence of free surfaces across which dislocations can leave the film. However, in these simulations the BE cannot be caused by the interaction between grains.

Indeed, in a 2D model of a film with a single layer of grains, there is essentially no interaction between grains: from a mechanical point of view, the film is a string of grains. In a real film, however, grains are 3D objects and there are also grains in the direction perpendicular to loading. Figure 5 shows a portion of a long film in a 3D view, with the highlighted cross-section being the area that we imagine to be represented in 2D. This figure emphasizes that the deformation of all grains in the 2D view needs to be accommodated by deformation of grains in front of and behind the plane of consideration. In other words, straining in the x_1 direction of any grain is constrained by all other grains; this is not accounted for in the 2D model so far. In order to avoid the complexity of 3D DDP, we will make the simple assumption that all grains in 2D have to co-deform with the others. In this so-called *constrained model*, all grains deform in the same way, as if they are mechanically in parallel. This is the opposite limit of the foregoing, uncon-

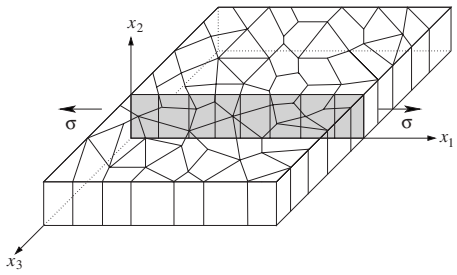

FIG. 5. Schematic of a columnar-grained thin film in 3D view. The gray section is what is addressed in a 2D film model.

strained model with all grains in series. We have implemented it by imposing the following constraint along the centers of the vertical GBs:

$$u_1(jd,h/2) = jd\varepsilon(t), \quad j = 1,2,\ldots,7, \tag{4}$$

(note that we use eight columns of grains in the periodic cell, see Fig. 1). In Fig. 6, the predicted BE using the constrained model of single-layer films is displayed. Comparing these results with the predictions of the unconstrained model, we note that the constraint tends to increase the BE, defined as $\varepsilon_B/\varepsilon_y$, for all films at any prestrain.

At the same time, the constraints are found to increase the hardening rate as well, as seen in Fig. 7 for $h=1$ and 0.34 μm columnar-grained films. As is clear from this figure, the constrained model (indicated by C) gives rise to a high hardening rate in comparison with the unconstrained model (denoted by U). This difference in hardening rates may suggest that the increase in the BE by the use of constraints is due to the increase in the hardening rate. To have a fair comparison between the obtained results of two models, we have decided to do a, so-called, refit: that is, to adapt the source density so that the stress-strain response of the constrained model coincides with the respective unconstrained response. In Fig. 7, the responses obtained with the refitted constrained model are also plotted (indicated by C-Rf). On average, the refit involves an increase in the density of sources by around 33%.

Figure 8 shows the predicted BE of columnar-grained films using the refitted constrained model. There is no significant difference between these results with the ones in Fig. 6, indicating that the increase in hardening rate by the introduction of constraints is not the main factor in determining the resultant BE. On the other hand, even though the loading responses are almost identical, the BE according to the refitted constrained model is systematically higher than that obtained by the unconstrained model in Fig. 4 (included as open symbols). This suggests that the additional out-of-plane constraint, introduced as a simple way to mimic the interaction between grains in a real film, is by itself responsible for an increase in the BE. Nevertheless, to eliminate the effect on hardening altogether, we will present the BE in the form of Fig. 3(c) in Sec. III B.

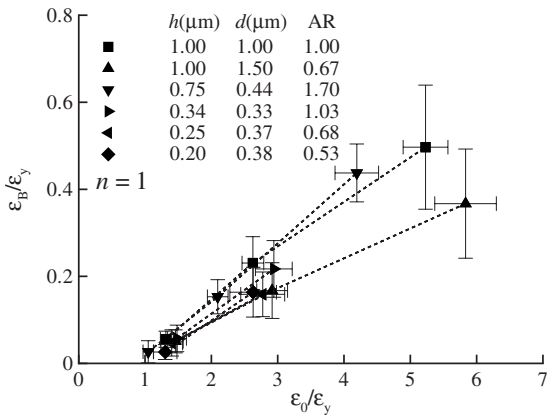

FIG. 6. ε_B as a function of ε_0 predicted for columnar-grained films by the constrained model. The corresponding unconstrained results are shown in Fig. 4.

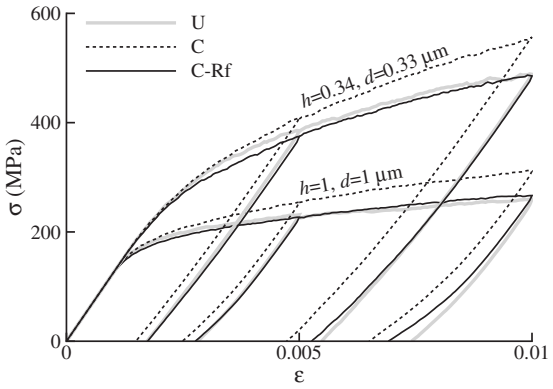

FIG. 7. Stress-strain curves of columnar-grained films using unconstrained model (indicated by U), constrained model (labeled by C) with the same model parameters used in unconstrained model, and constrained model by doing a refit to coincide on respective unconstrained response (indicated by C-Rf). For clarity, only the average response is plotted, without scatter.

Subsequently, Fig. 9 shows the predicted BE in multilayer films: (a) and (b) for the unconstrained model, while the results where the grains are constrained according to Eq. (4) are shown in (c) and (d). In contrast to columnar-grained films, the influence of the constraint is very small for multilayer films. The reason for this is that in multilayer films, the grains already interact rather strongly in the through-thickness direction; hence, the effect of grain interaction on the BE is naturally captured in such films.

Figure 10 confirms that the grains in multilayer films interact through the film thickness. The responses obtained using the constrained model are almost the same as those of the unconstrained model, both during loading and during unloading. Hence, there is no need to refit the response of the constrained model. In all the multilayer results presented here it should be kept in mind that while they highlight the role of GBs, there is also an effect caused by free surfaces. While GBs are more active in serving as barrier to dislocation motion in multilayer films than in columnar-grained ones, free surfaces from which dislocations can escape the film become relatively more important in films with columnar grains. A discussion of their distinct effect on the BE is postponed to the next section.

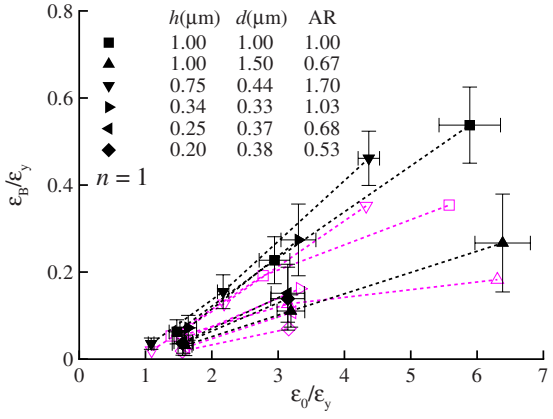

FIG. 8. (Color online) ε_B as a function of ε_0 predicted for columnar-grained films by the constrained model after a refit of the source density, see Fig. 7. The corresponding unconstrained results (open symbols) are superimposed from Fig. 4.

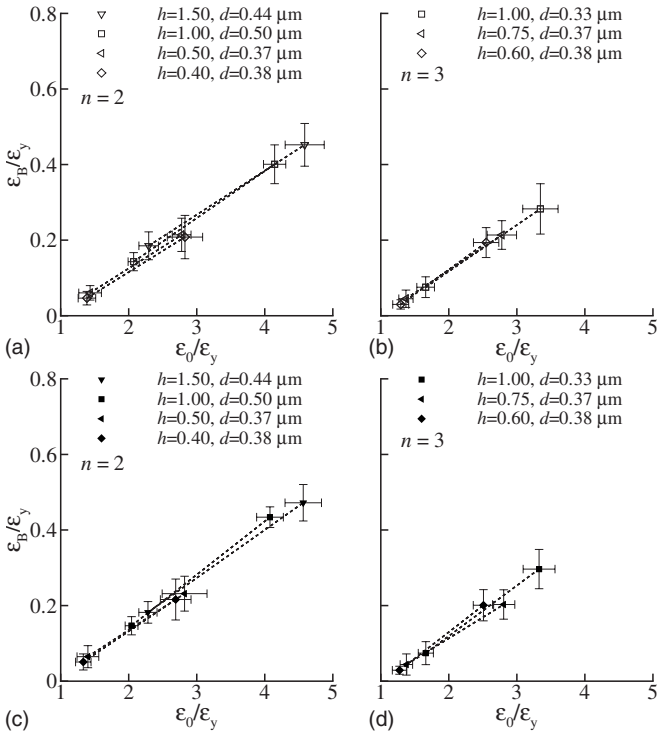

FIG. 9. ε_B as a function of ε_0 for multilayer films unloaded from $\varepsilon_0 = 0.005$ and 0.01. (a) and (b) Unconstrained model, and (c) and (d) Constrained model. Dashed lines are drawn as a guide to the eye.

Besides offering a simple way to incorporate grain interactions in single layer films, the constrained model tends to reduce statistical variations in the overall response among different realizations. This is observable in Figs. 4 and 8. Also, the statistical fluctuations in the predicted stress-strain response are smaller. Although, for clarity purposes, the scatter was not shown in Figs. 7 and 10, the scatter for the various realizations is shown in Fig. 11 for the predicted yield strength σ_y as a function of film thickness. The statistical fluctuations are clearly lower when using the constrained model, especially for films with columnar grains. Moreover, the yield strength of multilayer films is not affected by adding constraints, because, as mentioned above, grains already interact across the film thickness. It is worth noting though that single-layer films with pancakelike grains have more scatter in the yield strength compared to needlelike grains because the probability of localized plastic behavior is higher in those films.

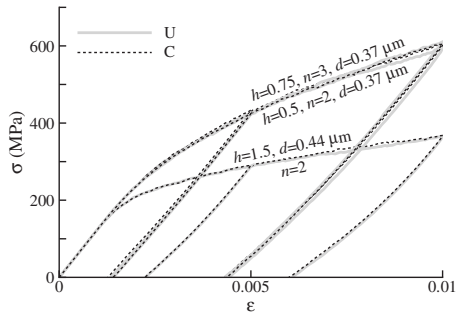

FIG. 10. Stress-strain curves for two- and three-layer films using unconstrained model (indicated by U) and constrained model (labeled C).

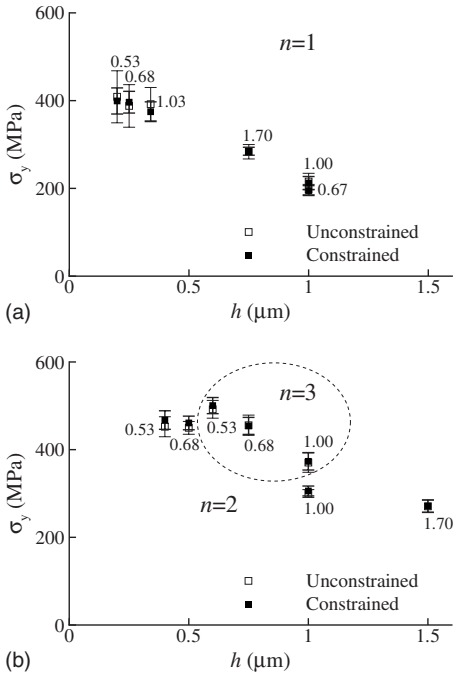

FIG. 11. Yield strength vs film thickness for (a) columnar-grained and (b) multilayer films. In the case of the single-layer films, the results of the constrained model with refitting are shown. The grain AR (see Table I) is indicated for each case.

B. Comparison with experiments

To make contact with experimental results in Ref. 2, Fig. 12 presents the results of the predicted ε_B for single- and

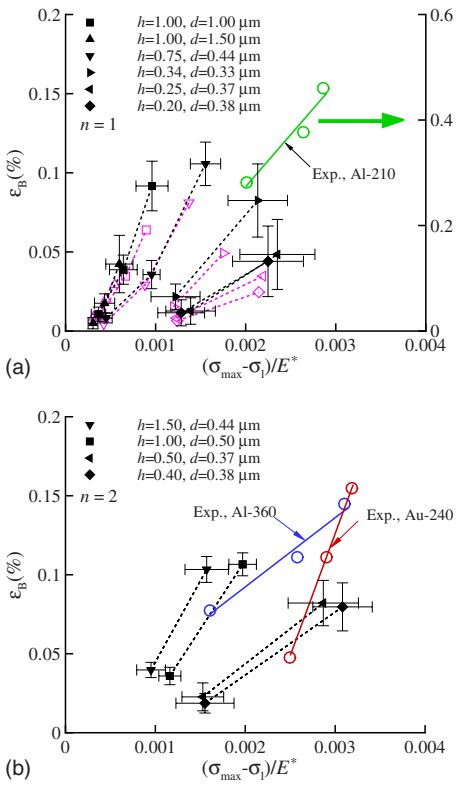

FIG. 12. (Color online) ε_B as a function of $(\sigma_{max} - \sigma_l)/E^*$ by using the constrained model. In (a), the results after refitting are shown together with the corresponding unconstrained results (open symbols). The experimental data are from Ref. 2. Dashed lines are drawn as a guide to the eye.

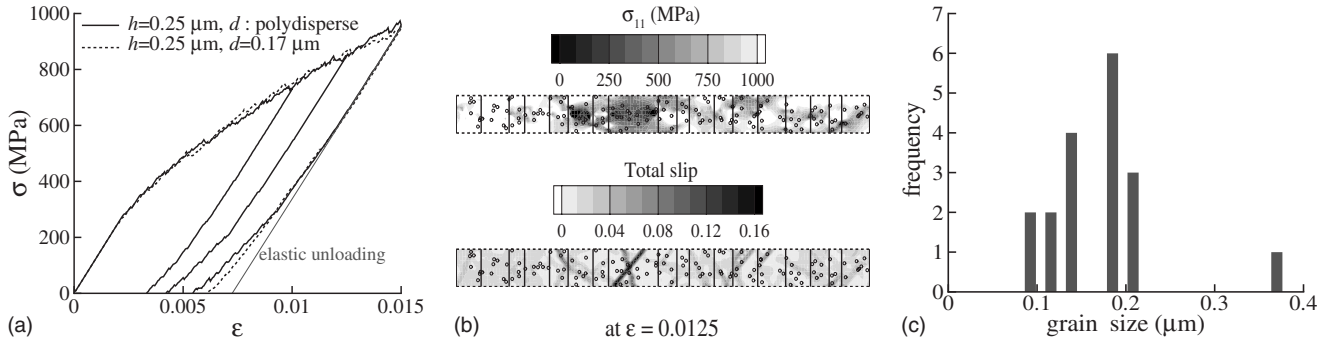

FIG. 13. (a) Stress-strain response of 0.25 μm thick film with columnar grains having different sizes. (b) Distribution of the tensile direction stress and the total slip at $\varepsilon=0.0125$, with the sources (circles) superimposed. (c) Grain size distribution in the computational cell, corresponding to an average of 0.17 μm. The response for this average grain size is shown in (a) with a dashed line, for comparison.

double-layer films (see Table I) as a function of $(\sigma_{\max}-\sigma_1)/E^*$ using the constrained model (note that for the single layer films, the refitted constrained model has been used). Rajagopalan *et al.*[2] reported measures of the BE in unpassivated freestanding Al and Au thin films with thickness in the range of 200 to 400 nm. Aluminum films, referred to as Al-210 have a thickness of $h=0.21$ μm and (average) grain size $d=0.17$ μm; Al-360 is a two-layer film with thickness $h=0.36$ μm and grain size $d=0.2$ μm. Gold films, named Au-240, with a thickness of $h=0.24$ μm have two grains across the thickness and grain size $d=0.08$ μm. The value of ε_B for Al-210 was reported to be around 0.4 %, while our predictions [Fig. 12(a)] for columnar-grained films with the material parameters specified above are always below ~0.1%; the possible reason for this discrepancy will be discussed later. The experimental results for Al-360 and Au-240 are included in the plot for two-layer films, Fig. 12(b). The agreement between predictions and experimental data is only qualitative, as is to be expected since the materials are different.

One of the mechanisms proposed by Rajagopalan *et al.*[2] to explain the BE in unpassivated thin films is based on the consideration that a polycrystalline film with random texture may contain large/favorably oriented grains that can deform plastically but are surrounded by small/unfavorably oriented grains that are effectively elastic. The resulting inhomogeneous stress distribution across grains will then contribute to a BE.

The objective of the following is to investigate such a mechanism with our present model. As reported in Ref. 2, the average grain size of Al-210 films is 0.17 μm, but there is a variation in grain size in the range of 0.05 to 0.4 μm. We have attempted to mimic these experimental conditions with a $h=0.25$ μm film with a grain size distribution as indicated in Fig. 13(c). The constrained model of this special film predicts a hardening rate in loading which is similar to that in a film with a uniform grain size of 0.17 μm [see Fig. 13(a)], but a stronger BE; after unloading from $\varepsilon_0=0.015$ the Bauschinger strain is ~50% higher when there is a dispersion of grain size. The stress distribution, shown in Fig. 13(b), is highly inhomogeneous and thus provides the preconditioning for reverse plasticity during unloading. The distribution of the total slip in the film shows that the large/favorably oriented grain carries most plastic strain and confirms that the small/unfavorably oriented grains remain mainly elastic.

The variation in ε_B with $(\sigma_{\max}-\sigma_1)/E^*$ for the 0.25 μm thick special film is displayed in Fig. 14(a). In this figure, the results of another realization are also shown, as well as those of two other special films but with $h=0.2$ μm. The computed values of the BE are similar to those reported for Al-210 in Ref. 2, see Fig. 14(a), but the dependence on prestress is somewhat weaker. However, these are two different materials with different elastic limits. Therefore, to get a more fair comparison, we normalize the strain $(\sigma_{\max}-\sigma_1)/E^*$ by the elastic limit strain, $\varepsilon_1:=\sigma_1/E^*$. The dependence of the BE on $[(\sigma_{\max}-\sigma_1)/E^*]/(\sigma_1/E^*)=(\sigma_{\max}-\sigma_1)/\sigma_1$, shown in Fig. 14(b), matches very well with the experimental data.

While the results shown in Fig. 13 are based on a DD model with many detailed constitutive rules, the basic feature

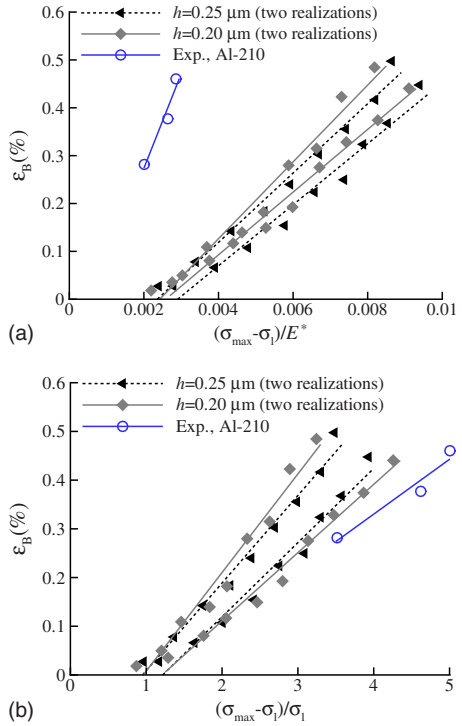

FIG. 14. (Color online) (a) ε_B vs $(\sigma_{\max}-\sigma_1)/E^*$ and (b) ε_B vs $(\sigma_{\max}-\sigma_1)/\sigma_1$. For comparison purpose, experimental data that has a similar polydispersity of grain size is also shown. The experimental data is from Ref. 2.

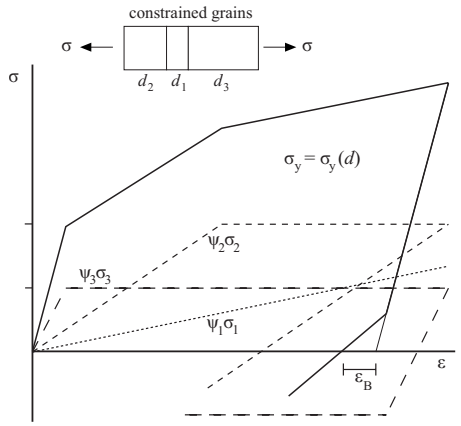

FIG. 15. Qualitative response of a constrained film model comprising three grains, with sizes $d_1 < d_2 < d_3$, each exhibiting size-dependent, perfect plasticity. The dashed lines represent the response of individual grains, multiplied by their respective volume fraction ψ. The overall response, shown as the solid curve, reveals a BE upon unloading as indicated.

of inhomogeneous stress on the grain level induced by enforcing homogeneous strain is akin to that of continuum polycrystalline models, such as the so-called full constraints Taylor model, or even the macroscopic so-called fraction model proposed by Besseling (see, e.g., Ref. 10). The latter model assumes that fractions of the material have different yield properties, and has proved to be successful in capturing the cyclic plastic response of engineering materials including the BE. In Fig. 15, we borrow the idea behind the fraction model to consider a "film" of three grains of the same height d_t but different widths $d_1 < d_2 < d_3$. Based on experimental findings[7] and DD results,[5] each grain is taken to have a yield strength that scales, qualitatively, in a Hall–Petch type manner with grain size. Hardening inside each grain is ignored for simplicity. When the grains are subjected to the same tensile strain (i.e., they deform in parallel), the response of individual grains is assumed to contribute to the overall in proportion with their volume fraction ψ (which in this simple model is equal to $d_i/\Sigma_j d_j$, $i=1,\ldots,3$). The resulting overall response of the film is the sum of the contributions $\psi_i\sigma_i$ of all grains. It is seen in Fig. 15 that this simple model—featuring grain interactions and size-dependent yield—is sufficient to capture a BE.

IV. DISCUSSION

In the foregoing section, the BE in a thin film is reported for a given material as a function of prestrain or prestress. Such plots are not suitable for a direct comparison of the BE in different films, since their properties are hidden. Classification of the size dependence of thin film BEs requires a characteristic measure of the film microstructure. In order to identify the appropriate one, we further explore the possible origins of the BE.

Since GBs generally serve as barriers for dislocation motion, dislocation pile-ups against GBs give a major contribution to hardening and likely to the BE. A scaling law between BE and the density of GBs can therefore be expected. For the limiting case of equally strained grains, the relation between the density of GBs and the BE for the various microstructures from Table I is, therefore, presented in Fig. 16(a) by plotting ε_B as a function of the density of GBs (defined as $\rho_{GB}^{(n)} = (1/d) + (n-1)/n(1/d_t)$ in Ref. 9). Linear fits are shown for films with the same number of layers, at prestrains of 0.005 and 0.01.

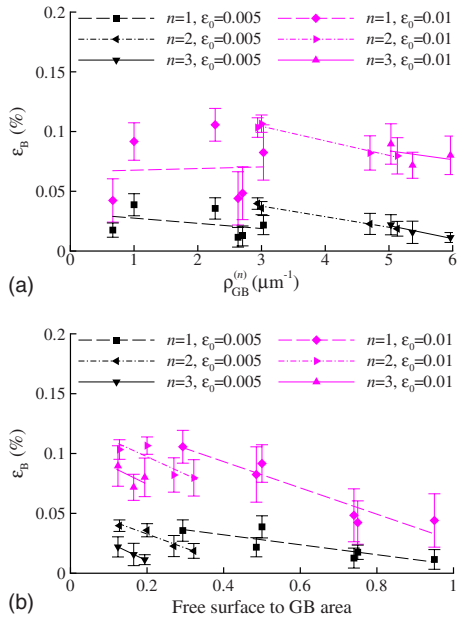

FIG. 16. (Color online) (a) ε_B as a function of "density of GB" and (b) ε_B as a function of "free surface to GB area." For definitions, see Table I.

From this figure, two observations are made. First, the correlation between ε_B and $\rho_{GB}^{(n)}$ is not as good as that between yield strength and GB density as reported by Kumar *et al.*[9] The data for single-layer films, in fact, do not even reveal a trend. The latter can be attributed to the fact that for $n=1$ the GB density parameter lacks any information about the film thickness and thus makes it hard to compare films with different thickness. Also, for such films, we have learned from Fig. 7 that for a given density of GBs, the BE increases with increasing constraint between grains, even when hardening is kept constant. Second, we see that whatever the film microstructure (i.e., value of n), the BE tends to decrease with increasing density of GB. These observations make us conclude that GB density is not the best measure to classify the BE.

The presence of GBs is not the only reason for stress inhomogeneity in unpassivated films; another origin resides in the presence of free surfaces from which dislocations can escape and by that enhance plastic flow of surface grains. As these grains may be surrounded by small/unfavorably oriented grains, the stress inhomogeneity in the film is enhanced. Therefore, Rajagopalan *et al.*[2] have suggested to use the ratio of free surface to GB area as a measure on which the BE depends. To study this explicitly, the computed Bauschinger strains are plotted versus the ratio of free surface to GB area (defined as $d/[2h+(n-1)d]$ in Ref. 2) in Fig. 16(b). Although the correlation is not always statistically significant for small values of the free surface to GB area ratio, there is a clear trend that a decrease in this ratio (either by decreasing the free surface or by increasing the GB area) leads to an increase in BE.

It should be noted that films with a polydisperse grain size have an additional intrinsic component of stress inhomogeneity that adds to that of GB and free surfaces; they are therefore excluded from Fig. 16.

V. CONCLUSIONS

2D DDP simulations have been employed to study the BE in single- and multilayer unpassivated films with thickness and grain size in the (sub)micrometer region. The underlying material model, incorporating the nucleation and glide of dislocations on multiple slip systems, provides an accurate description of the size-dependent behavior of thin films under monotonic loading. In the present simulations of thin films under cyclic loading, the BE can originate from various mechanisms: dislocation pile-ups against GBs; constraints on the grain level by neighboring grains; variations in grain orientation; polydispersity of the grain size. All of these control the level of stress inhomogeneity inside the films; it is this inhomogeneity that eventually is the driving force of the BE.

The salient conclusions of this study are:

- the prediction of a realistic BE in thin films requires that the interaction between grains is taken into account;
- this interaction is included naturally in multilayer grains, and can be incorporated in a simple, approximate manner by imposing affine-strain constraints per grain;
- accounting for a polydisperse grain size is necessary for a realistic prediction of the BE and for a quantitative agreement with experimental findings, as hypothesized in Ref. 2;
- the BE increases with a decreasing aspect ratio of grain height over grain width;
- the ratio of free surface to GB area, as suggested in Ref. 2, is a useful measure to classify the BE in unpassivated thin films.

Even though being 2D, the model is able to capture all BE phenomena in thin films observed experimentally so far.

ACKNOWLEDGMENTS

SSS gratefully acknowledges financial support from the Ministry of Science, Research, and Technology of Iran for his scholarship at the University of Groningen.

APPENDIX A: SIZE-DEPENDENT SOURCE STRENGTH DISTRIBUTION

In the grain size dependent source strength model, the strength τ_{nuc} of each source is to be determined from Eq. (3), as mentioned in Sec. II. The part $\tau_{\mathrm{nuc}}^{\mathrm{LN}}$ of the source strength is picked randomly from a log-normal distribution as shown schematically in Fig. 17. As described in detail in Ref. 5, the distribution is bounded from below by the strength of a source with maximum available length in the grain. The maximum source length in a tetragonal grain with grain size d and height d_{t} (see Fig. 1) is

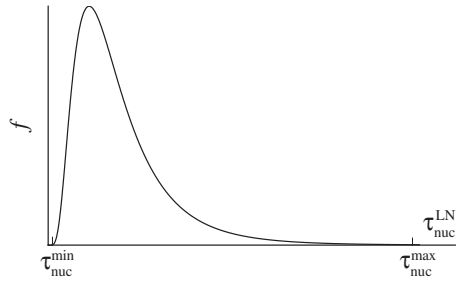

FIG. 17. Log-normal distribution of source strengths.

$$l_{\mathrm{FR}}^{\mathrm{max}} = \sqrt{d_{\mathrm{t}}^2 + 2d^2},$$

and the associated strength is

$$\tau_{\mathrm{nuc}}^{\mathrm{min}} = \beta_{\mathrm{nuc}} \frac{\mu b}{l_{\mathrm{FR}}^{\mathrm{max}}},$$

where the parameter β_{nuc} depends on Poisson's ratio ν, the inner cut-off radius and the line character. The maximum value of the source strength in the distribution is defined to be the theoretical shear strength of the material,

$$\tau_{\mathrm{nuc}}^{\mathrm{max}} = \tau^{\mathrm{th}},$$

which for Cu is $\mu/18$. The parameters needed to define the distribution are determined by the method proposed in Ref. 5. As mentioned in Sec. III, the approach implies that the density of potential dislocation sources, ρ_{nuc}, scales inversely proportional to the grain size d. The latter is a consequence of the assumption that the length of the underlying 3D Frank–Read segment scales with the grain size and that a 2D model of a film (see Figure 5) captures $1/d$ number of grains per unit out-of-plane width. Yet, the minimum number of sources is determined by the condition that the log-normal distribution is sampled with a 90% confidence level.

[1] Y. Xiang and J. J. Vlassak, Acta Mater. **54**, 5449 (2006).
[2] J. Rajagopalan, J. H. Han, and M. T. A. Saif, Scr. Mater. **59**, 737 (2008).
[3] R. Fertig and S. P. Baker, Prog. Mater. Sci. **54**, 874 (2009).
[4] L. Nicola, Y. Xiang, J. J. Vlassak, E. Van der Giessen, and A. Needleman, J. Mech. Phys. Solids **54**, 2089 (2006).
[5] S. S. Shishvan and E. Van der Giessen, J. Mech. Phys. Solids **58**, 678 (2010).
[6] E. Van der Giessen and A. Needleman, Modell. Simul. Mater. Sci. Eng. **3**, 689 (1995).
[7] P. A. Gruber, J. Böhm, F. Onuseit, A. Wanner, R. Spolenak, and E. Arzt, Acta Mater. **56**, 2318 (2008).
[8] R. Kumar, F. Székely, and E. Van der Giessen, "Modelling dislocation transmission across tilt grain boundaries in 2D," Comput. Mater. Sci. (in press).
[9] R. Kumar, L. Nicola, and E. Van der Giessen, Mater. Sci. Eng., A **527**, 7 (2009).
[10] J. F. Besseling and E. Van der Giessen, *Mathematical Modelling of Inelastic Deformation* (Chapman and Hall, London, 1994).